Materials and Design 193 (2020) 108791

Contents lists available at ScienceDirect

Materials and Design

journal homepage: www.elsevier.com/locate/matdes

Self-assembly of graphene oxide and cellulose nanocrystals into continuous filament via interfacial nanoparticle complexation

Kaitao Zhang [a], Lukas Ketterle [b], Topias Järvinen [c], Gabriela Simone Lorite [c], Shu Hong [d,a], Henrikki Liimatainen [a,*]

[a] Fiber and Particle Engineering Research Unit, University of Oulu, P.O. Box 4300, FI-90014, Finland
[b] Institute for Mechanical Process Engineering and Mechanics, Faculty of Chemical and Process Engineering, Karlsruhe Institute of Technology, 76344 Eggenstein-Leopoldshafen, Germany
[c] Microelectronics Research Unit, Faculty of Information Technology and Electrical Engineering, University of Oulu, P.O. Box 4300, FI-90014, Finland
[d] College of Materials Science and Engineering, Nanjing Forestry University, Nanjing 210037, China

HIGHLIGHTS

- Cellulose nanocrystals and graphene oxide hybrid filaments were fabricated.
- Interfacial nanoparticle complexation method was applied to draw hybrid filament.
- Conductive hybrid filament was obtained after chemical reduction.

GRAPHICAL ABSTRACT

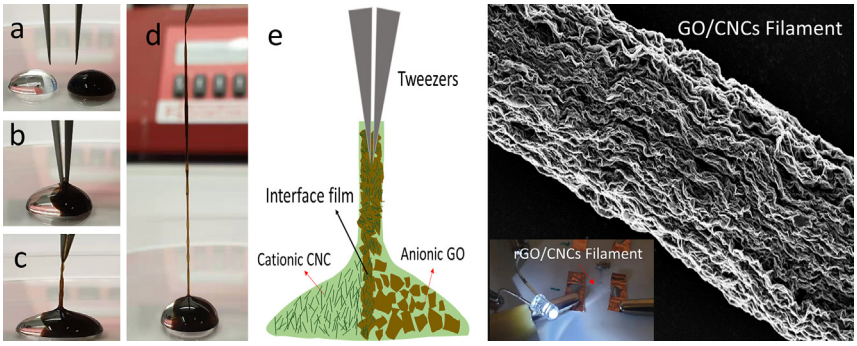

ARTICLE INFO

Article history:
Received 12 April 2020
Received in revised form 4 May 2020
Accepted 5 May 2020
Available online 11 May 2020

Keywords:
Nanocellulose
Graphene oxide
Filament
Interfacial complexation

ABSTRACT

The present work demonstrates the spinning of conductive filaments from oppositely charged nano-scale entities, i.e., cationic cellulose nanocrystals (CNC) and anionic graphene oxide (GO), via interfacial nanoparticle complexation. Especially, the role of CNC and GO concentration in filament formation was investigated. Moreover, the chemical structure, morphology and composition of formed CNC/GO composite filaments were further characterized. The positively charged CNC formed firstly a complex film with negatively charged GO flake and then the complexed structures were further assembled into macroscale hybrid filament (diameter about 20 to 50 μm). After chemical reduction of the hybrid filament, conductive filaments with an average tensile strength of 109 ± 8 MPa and electrical conductivity of 3298 ± 167 S/m were obtained. The presented approach provides a new pathway to understand the interaction of GO and nanocellulose, and to design macroscopic, assembled and functionalized architectures of GO and nanocellulose composites.

1. Introduction

Graphene, consisting of several single layers of carbon atoms arranged in a honeycomb lattice, has received much interest due to its outstanding electronic, thermal, and mechanical properties and potential applications in optoelectronics [1], energy-storage [2], and sensors

* Corresponding author at: Fiber and Particle Engineering Research Unit, University of Oulu, P.O. Box 4300, FI-90014, Finland.
E-mail addresses: kaitao.zhang@oulu.fi (K. Zhang), topias.jarvinen@oulu.fi (T. Järvinen), gabriela.lorite@oulu.fi (G.S. Lorite), henrikki.liimatainen@oulu.fi (H. Liimatainen).

https://doi.org/10.1016/j.matdes.2020.108791

[3]. Particularly, graphene oxide (GO), as one of the most important derivatives of graphene, is a negatively charged and oxygen-functionalized form of graphene produced from chemical exfoliation of graphite [4]. The multiple oxygen-containing functional groups, such as epoxy, hydroxyl, and carboxylic acid, on the basal planes and edges of GO sheets significantly improve the dispensability of GO in polar solvents [5]. To promote the practical application of graphene, the integration of individual graphene nanosheets into ordered macroscopic materials becomes crucial [6]. Thus, various graphene based macroscopic materials such as films [7,8], aerogels [9,10], hydrogels [11] and fibers [12–14] have been fabricated via self-assembly of graphene and its derivatives. The obtained macroscopic materials usually own hierarchical microstructures with superior properties translated from the inherent attributes of graphene [15]. Graphene fiber (GF) has arisen high expectations as new carbonaceous fibrous materials in terms of mechanical and functional performance since it was first prepared by the wet spinning of graphene oxide (GO) [16]. By virtue of the electrical conductivity, flexibility, toughness, and strength of GFs, some potential applications of GFs have been demonstrated including conducting wires, fiber-shaped energy-storage devices, and sensors [17–20].

Nanoscale building blocks from biological origin have attracted tremendous interest in materials science and engineering [21]. As natural nanomaterial produced from native cellulose including plants, animals, and bacteria, nanocellulose (NC, usually referring to cellulose nanofibers (CNF), cellulose nanocrystals (CNC) or bacteria cellulose fibers), possesses many characteristics similar with graphene, such as large specific surface area, excellent mechanical properties, and tailorable surface chemistry. On the other hand, it also holds many appealing features different from graphene like high crystallinity, biodegradability and renewable resource [22]. Recently, many researchers have been attempting to combine NC with graphene to assemble multifunctional hybrid composites, which possess the advantages of both NC and graphene [23–27]. Various hybrid composites of NC and graphene have been fabricated, such as films, aerogels and filaments [28–31] and they have been used in water treatment, supercapacitors and sensors [32–34]. Most of the assembled materials target to membranes or aerogels, and only a few efforts on designing of macroscopic NC and graphene hybrid filaments have reported.

The micro-sized CNF and GO hybrid (NC/GO) filaments with a noticeable improvement in mechanical properties were firstly fabricated by Li et al. [30,35]. The fabricated NC/GO filaments were successfully used as high performance fiber-shaped supercapacitors. The hydrophilic NC can act as a "spacer" to effectively reduce π-π stacking interactions between the graphene and facilitate the absorption of electrolyte, improving the electrochemical performance of the supercapacitors [36–39]. However, most of these reported NC/GO hybrid filaments were prepared by traditional wet-spinning method, in which volatile organic coagulation solvents and repeated washing processes are needed. In our previous paper, we reported a mild and green method to fabricate micro-sized fibers from oppositely charged nanoparticles using interfacial nanoparticle complexation (INC). This method was carried out under aqueous conditions at neutral pH and at room temperature based on oppositely charged one-dimensional (1D) CNF and CNC [40,41]. As mentioned before, GO is a colloidal negatively charged nanoflake with carboxylic groups on its surface. Moreover, the complexation of GO with polyelectrolytes (such as chitosan) into mesoscale fiber was also demonstrated [42–44]. Given these fact, there is a strong possibility that negatively charged GO could complex with positively charged NC to fabricate NC and GO (NC/GO) filament based on INC method. Different from the complexation with soluble polyelectrolytes, the INC complexation reported here is between two non-soluble charged nanomaterials, i.e., two dimensional (2D) GO nanosheets and 1D CNCs, which may broaden the suitable materials for the INC complexation (from 1D with 1D to 1D with 2D).

Herein, two types of positively charged CNCs were prepared and used to complex with negatively charged GO to assemble CNC and GO hybrid filaments. Especially, CNC/GO composite filaments with variable CNC and GO concentrations were investigated. Moreover, the chemical structure, morphologies and composition of formed CNC/GO composite filaments were further characterized. After chemical reduction of the obtained hybrid filament, conductive reduced GO filament was obtained, showing good mechanical properties and an electrical conductivity of 3298 ± 167 S/m.

2. Materials and methods

2.1. Materials

Bleached kraft birch (*Betula pendula*) commercial pulp sheet was used as a source of cellulose. Lithium chloride (LiCl, 99%), sodium periodate ($NaIO_4$) and glycerol were acquired from Sigma Aldrich (Germany). Girard's reagent T (2-hydrazinyl-2-oxoethyl)-trimethylazanium chloride (GT), aminoguanidine hydrochloride (AH) and hydroiodic acid (HI) were supplied from Tokyo Chemicals Industry (Japan). Graphene oxide (GO) was purchased from NewMater Nanotech (Sichuang, China) in a water solution of 10 mg/ml and used without further purification. Deionized water was used in all experiments.

2.2. Methods

2.2.1. Preparation of 2,3-dialdehyde cellulose (DAC) by periodate oxidation

15.0 g of bleached birch pulp was torn and mixed at 10000 rpm with 1500 ml deionized water using an Ultra-Turrax mixer (IKA T25, Staufen, Germany) for 1 min. Then, 12.3 g of $NaIO_4$ and 27 g of LiCl were added into the dispersion and the reaction was conducted at 65 °C in a water bath for 3 h with an aluminum foil cover. After reaction, the product was filtered and washed several times with deionized water and stored in a non-dried state at 4 °C for further use [45]. The aldehyde content of DAC was measured to be 3.86 mmol/g based on an oxime reaction between the aldehyde group and $NH_2OH{\cdot}HCl$ [46].

2.2.2. Cationization of DAC with Girard's reagent T or aminoguanidine hydrochloride

Cationization of DAC was conducted using two different routes as described previously [45,47,48]. Reaction routes are shown in the Fig. S1 in Supplementary Information.

2.2.2.1. Cationization of DAC with Girard's reagent T. 24.32 g of Girard's reagent T was firstly dissolved to 600 ml of deionized water in a beaker and the pH of solution was adjusted to 4.5 using a dilute HCl. 6.0 g of non-dried DAC was added and the mixture was stirred and allowed to proceed for 72 h at room temperature [48]. After that, the product was purified by water filtration until the conductivity of the filtrate was below 20 μS cm^{-1}.

2.2.2.2. Cationization of DAC with aminoguanidine hydrochloride (AH) in deep eutectic solvent (DES) system. The DES system was synthesized by mixing of aminoguanidine hydrochloride (75 g) and glycerol (125 g) with a molar ratio 1:2 into a flask and preheated to 90 °C. After the mixture became a transparent liquid, it was cooled down to 80 °C. Then, 10 g (abs.) non-dried DAC was added into DES liquid for reaction. The mixture was stirred continuously by magnetic bar and reacted for 10 min. The reaction was stopped by adding 250 ml of ethanol. The obtained product suspension was filtrated and washed twice with 500 ml of water and ethanol, respectively [47].

2.2.3. Nanofibrillation of cationic cellulose pulps to CNC

The chemically treated cationic cellulose pulps were passed through a double-chamber system (400 and 200 μm) of a microfluidizer (Microfluidics M-110EH-30, USA) for two times at 1000 bar pressure using a solids content of 1 wt%. The cationic CNC obtained from DAC

reaction with GT and AH were denoted as GT-CNC, and AH-CNC, respectively.

2.2.4. CNC/GO filament fabrication

Droplets of oppositely charge GO and CNC aqueous suspensions (100 μL each) were placed adjacent to each other on a polystyrene Petri dish without the two droplets coming into together. Then, a pair of tweezer was plunged into the two droplets to bring them into contact to form a stable interface. The plunged tweezer was further clamped to the universal testing machine and dragged upwards with a constant rate of 30 mm/min, resulting in the formation of a continuous filament (Video.S1). All formed wet filaments were attached to a glass rod and air-dried at room temperature. The hybrid filaments formed by GT-CNC or AH-CNC with GO was designated as GT-CNC/GO filament and AH-CNC/GO filament, respectively.

2.2.5. Reduction of AH-CNC/GO filament

The formed AH-CNC/GO hybrid filaments were immersed into HI solution (57 wt%) at 80 °C for 6 h, washed with water and ethanol to remove the HI and iodine, and finally dried at 80 °C under vacuum for 12 h to obtain AH-CNC/reduced GO (rGO) hybrid filaments.

2.2.6. Transmission electron microscopy

The morphological features of cationic CNC and GO were measured by transmission electron microscope (TEM, JEOL JEM-2200FS, Japan). Preparation of the samples was performed by first adding a small droplet of 0.003 to 0.005 wt% CNC suspension on the top of carbon-coated copper grid. After setting for 1 min, the sample was absorbed by a small piece of filter paper, the sample left on the grid was negatively stained with uranyl acetate (2% *w*/*v*) for 1 min. The staining agent was then removed again by filter paper. All the samples were allowed to dry at room temperature before the measurements were conducted. The standard conditions with 200 kV were used during the TEM analysis. The dimensions of the CNC were measured (>100 individual particles) using iTEM (Olympus Soft Imaging Solutions GMBH, Munster, Germany) image analysis software.

2.2.7. Atomic force microscopy imaging

The morphology of GO was analyzed by an atomic force microscope (AFM, MultiMode8, Bruker, Germany) with ScanAsyst™ in air and triangular Si probes (with a typical tip radius of 2 nm and a nominal spring constant of 0.4 N/m). 30 μL of 0.001% *w*/w GO dispersion was dripped on a freshly cleaved mica surface after 1 min bath sonication and air-dried for the analysis.

2.2.8. Field emission scanning electron microscope

The structure of formed filaments were observed using a field emission scanning electron microscopy (FESEM, Zeiss Sigma HD VP, Oberkochen, Germany) at 0.5 kV acceleration voltage. All samples were sputtered with platinum prior to observation.

2.2.9. Elemental analysis

The cationic group content of GT-CNC and AH-CNC were calculated directly from the nitrogen content of the product as determined using a PerkinElmer CHNS/O 2400 Series II elemental analyzer. The content of cationic CNC in the formed hybrid filament were calculated based on the equation below:

$$\text{CNC content (wt\%)} = \frac{\textit{Nitrogen wt\% of CNC/GO hybrid filament}}{\textit{Nitrogen wt\% of cationic CNC}} \times 100.$$

2.2.10. Polyelectrolyte titration

The charge density of GO was determinated by a particle charge detector (Mütek PCD 03, USA), in which 10 ml 0.01 wt% GO was titrated with poly-diallyl-dimethylammonium-chloride (polyDADMAC 1 meq/L) and the charge density was calculated based on the consumption of polyDADMAC (see the calculation equation in the Supplementary Information). The results are the average of at least three tests with minor difference.

2.2.11. Diffuse reflectance infrared Fourier transform spectroscopy

The chemical characterization of cationic CNC, GO and the formed composite filaments were carried out using diffuse reflectance infrared Fourier transform (DRIFT). The spectra were recorded on a Bruker Vertex 80v spectrometer (USA) in the 800–4000 cm^{-1} range with 2 cm^{-1} resolution.

2.2.12. Mechanical properties

The tensile tests of the filaments were performed on a universal testing machine (Zwick D0724587, Switzerland) equipped with a 200 N load cell. The filaments were preconditioned at room temperature (23 °C) and a relatively humidity of 50% for at least one day prior to the testing. All the samples were tested at a speed of 5 mm/min at room temperature and a gauge length of 20 mm using a pre-force of 0.01 N until breakage. The diameters of fibers were measured with an optical microscope (Leica MZ6 equipped with a Leica DFC420 camera) and the cross-section was assumed to be circular. A total of 5–6 measurements for each sample were tested, and their average value was reported.

2.2.13. Electrical conductivity measurement

Current-voltage (*IV*) -curves of reduced CNC/rGO hybrid filaments were measured using a two-point probe setup (Keithley 2636A sourcemeter, 21 °C at 30% relative humidity). The filaments were fixed with silver paste which was also used as a contact point for the probes. When calculating the electrical conductivity, the filament was regarded as a perfect round shape. A Leica DM2700 microscope was used to measure the length and diameters of dried filaments. Six samples were prepared and each sample was analyzed for three times, and the values with large errors in each measurement were excluded. Electrical conductivity is calculated based on this formula: $\sigma = 1/\rho = L/RA = LI/VA$, ρ is the resistivity; V is the voltage; I is the current; R is resistance; L is the fiber length; and the cross-section of fiber is regarded as round shape and A is the cross-section area calculated from diameter.

3. Results and discussion

3.1. Morphology of GT-CNC, AH-CNC and GO

Cationic CNCs were prepared based on our previously reported methods [47–49]. The chemical pretreatment of cellulose provides cationic charged groups on the surface of cellulose fiber, which would facilitate the nanofibrillation of cellulose pulp by the strong shear forced caused by the mechanical disintegration [49,50]. Fig. 1a-c show the morphologies of GT-CNC, AH-CNC and GO as characterized by TEM and Fig. 1d is the AFM image of GO. The obtained GT-CNC consisted of rod-like nanocrystals of 92 ± 28 nm in length and 6 ± 1.5 nm in width (Fig. 1a). AH-CNC prepared in DES system displayed a similar morphology with 92 ± 31 nm in length and a diameter of 6.6 ± 1.4 nm (Fig. 1b). The size distributions of CNC can be found in Fig. S2. GO showed smooth, transparent and flake-like appearance (Fig. 1c). The elastic wrinkles and the scrolled or folded edges were also observed as darker areas. The average dimension and thickness of GO were obtained using AFM imaging (Fig. 1d and Fig.S3). The dimensions of GO sheets varied from hundreds of nanometers to around 8 μm and the thickness was about 1 nm, corresponding to a single layer structure.

3.2. Feasibility of GT-CNC/GO and AH-CNC/GO in filament drawing

The amount of cationic groups in GT-CNC and AH-CNC were determined to be 1.1 and 2.3 mmol/g, respectively, using elemental analysis.

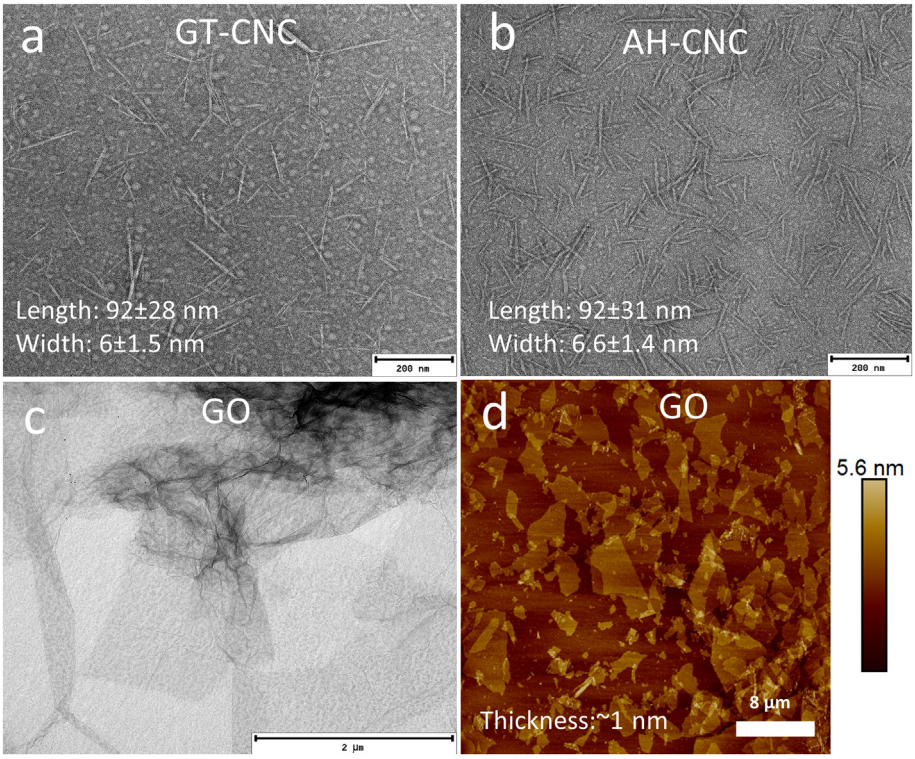

Fig. 1. TEM image of (a) GT-CNC, (b) AH-CNC and (c) GO and AFM image of GO.

The anionic charge density of GO was in turn 0.39 mmol/g as measured with polyelectrolyte titration. When the GT-CNC or AH-CNC suspension was mixed with GO suspension, precipitated complexes formed immediately owning to the ionic complexation of oppositely nanoparticles, presumably attributed to interaction between carboxyl groups for GO and quaternary ammonium groups of GT-CNC or AH-CNC (Fig. 2a).

INC method was used to form continuous CNC/GO hybrid filament from aqueous droplets of CNC and GO as is illustrated in Fig. 2b-e. By combining the two droplets of oppositely charged nanoparticle suspensions together using a pair of tweezers, self-standing GT-CNC/GO and AH-CNC/GO filaments could be successfully drawn. It is hypothesized that a complex film of CNC and GO formed immediately on the contact interface of droplets, and by picking up the interface film upwards, continuous hybrid filament of CNC and GO could be drawn (Fig. 2g).

The influence of GT-CNC, AH-CNC and GO concentrations on composite filament drawing process was studied using a constant drawing

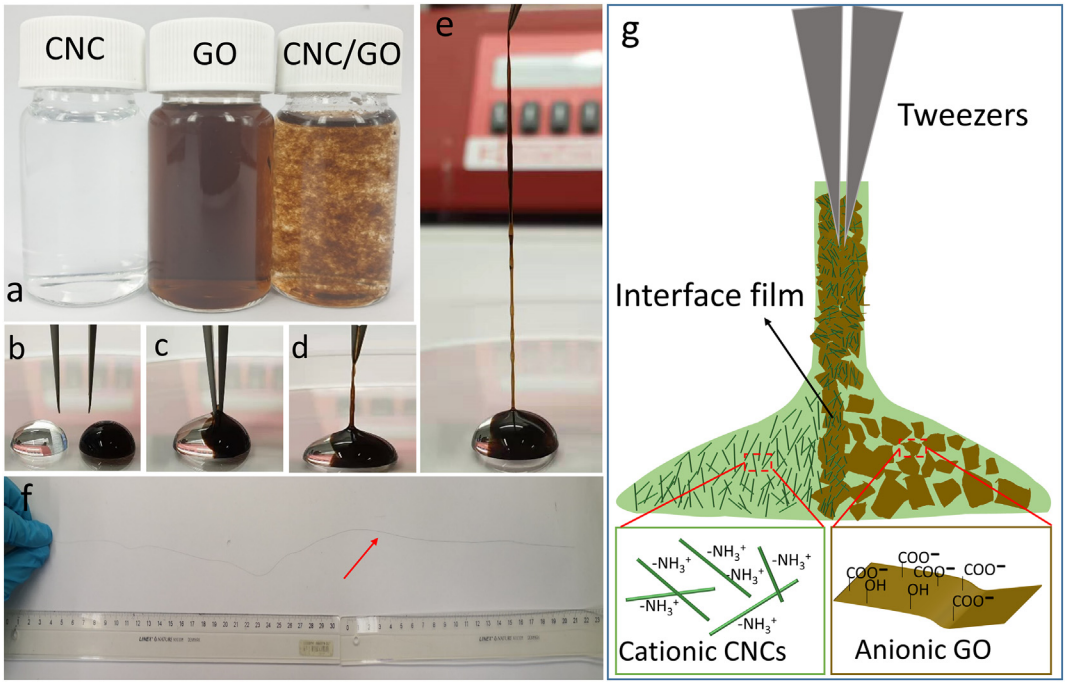

Fig. 2. (a) Suspensions of cationic CNC and GO and a dual precipitated complex after simple mixing; (b-e) CNC/GO hybrid filament drawing process; (f) a single dry CNC/GO hybrid filament with a diameter of ~ 33 μm and a length of 53 cm; (g) a scheme illustrating the CNC/GO hybrid filament drawing process.

Table 1
Effects of concentrations of GT-CNC, AH-CNC and GO on the CNC/GO hybrid filament formation and diameter of filaments.

Sample	0.5 wt% GO	0.3 wt% GO	0.15 wt% GO	0.05 wt% GO
0.5 wt% GT-CNC	51 ± 10 μm	36 ± 5 μm	30 ± 3 μm	NO
0.3 wt% GT-CNC	35 ± 7 μm	24 ± 3 μm	23 ± 2 μm	NO
0.15 wt% GT-CNC	34 ± 2 μm	20 ± 2 μm	16 ± 2 μm	NO
0.5 wt% AH-CNC	50 ± 8 μm	46 ± 6 μm	32 ± 4 μm	NO
0.3 wt% AH-CNC	43 ± 5 μm	36 ± 5 μm	23 ± 5 μm	NO
0.15 wt% AH-CNC	32 ± 3 μm	26 ± 3 μm	20 ± 2 μm	NO

speed of 30 mm/min. The formed filaments were dried in room temperature and their diameters were measured using an optical microscope. It was observed that the GO suspensions from 0.15 to 0.5 wt% formed uniform and strong filaments with 0.15 to 0.5 wt% GT-CNC or AH-CNC suspensions (Table 1). When the concentration of GO decreased to 0.05 wt%, the filament was too weak to be drawn upward. The diameter of the formed CNC/GO hybrid filaments decreased with decreasing the concentration of GO or CNC suspension. Using 100 μL droplet of 0.3 wt % AH-CNC or GT-CNC with 100 μL 0.3 wt%, CNC/GO, uniform filaments with a length higher than 60 cm could be obtained.

3.3. DRIFT

Diffuse reflectance infrared Fourier transform (DRIFT) spectroscopy was used to confirm the presence of GO, GT-CNC or AH-CNC in the formed INC filaments. Fig. 3 depicts the DRIFT spectra of GO, GT-CNC, AH-CNC and their corresponding hybrid filaments. In the spectrum of GO, the absorbance bands at 3434, 1743, 1620 and 1074 cm^{-1} can be attributed to the O—H stretching, C═O of carboxyl group, aromatic C═C bond in unoxidized graphitic domain and the C—O stretching in epoxy group, respectively [51]. The typical characteristic peaks of cellulose could be observed in all cellulosic samples (GT-CNC, AH-CNC and their hybrid filaments). The broad bands near to 3405 cm^{-1} were related to hydroxyl group stretching vibration while the band at 2904 cm^{-1} is associated with the C—H stretching vibrations in the cellulose glucose rings. It can be observed that GT-CNC exhibited a distinctive band between 1600 and 1700 cm^{-1} (mainly overlapping of C═O and C═N stretching) and amide II band at 1550 cm^{-1} (C—N stretching coupled with N—H bending modes) [52]. In the spectrum of AH-CNC, two obvious peaks at 1681 and 1641 cm^{-1}, corresponding to the C═N bond vibration and N—H bond bending, respectively, were also observed. The carboxyl group of GO (1743 cm^{-1}) was found in GT-CNC/GO and AH-CNC/GO filaments, but it shifted to a lower peak at 1737 cm^{-1},

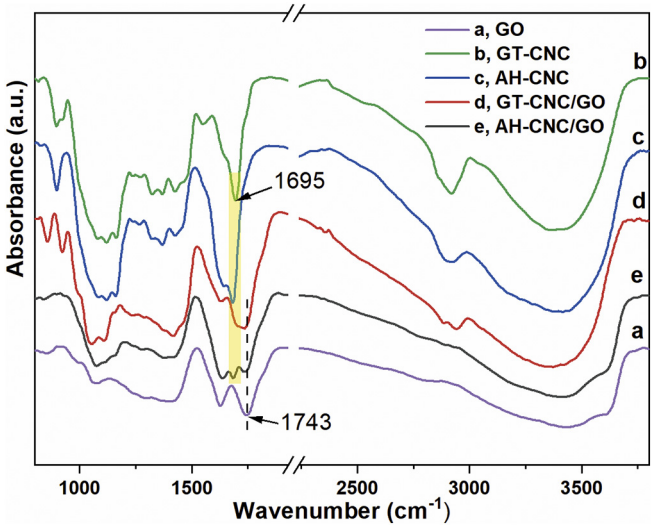

Fig. 3. DRIFT spectra of GO, GT-CNC, AH-CNC and their corresponding hybrid filaments.

indicating the successful incorporation of GO into the CNC/GO filament. In addition, the carbonyl band (1695 cm^{-1}) of GT-CNC and the C═N band (1681 cm^{-1}) of AH-CNC slightly shifted to 1702 and 1683 cm^{-1}, respectively, which probably due to the ionic bonding between the carboxyl group of GO and quaternary ammonium group of GT-CNC or AH-CNC.

3.4. Morphology of formed GT-CNC/GO and AH-CNC/GO filaments

The surface and cross sectional morphologies of obtained hybrid filaments are shown in Fig. 4. Various wrinkles and gullies could be observed aligned along the longitudinal direction of the formed filaments. Interestingly, the rod-like CNC which was randomly distributed on the surface of GO flakes, could be observed on surface of both hybrid filament at higher magnification (Fig. 4c and f), (More SEM images can be found in Fig.S4 and S5 in Supplementary Information). Moreover, more CNCs were found on the surface of GT-CNC/GO than that of AH-CNC/GO filament, probably indicating more GT-CNC was incorporated into the hybrid filament. The cross sectional area of formed CNC/GO filaments is presented in Fig. 4 d-f (GT-CNC/GO) and j-l (AH-CNC/GO). The hybrid filaments displayed a circular cross-section, this structure was probably associated with the supporting effect of CNCs on GO skeleton [36]. Layered structures of curvy GO flakes were revealed in the cross sectional area, which were stacked compactly and parallel to the axial direction. However, no CNCs was found in the cross-sectional area. Based on these microstructural findings, Fig. 4m presents a possible structure of formed CNC/GO hybrid filament. This structure was created when the positively charged CNC firstly complexed with GO flakes and the individual complexes further assembled into macroscale layered hybrid filament.

3.5. Composition of CNC/GO filaments

Elemental analysis was conducted to determine the composition of CNC/GO hybrid filament fabricated using 0.3 wt% CNC (GT-CNC or AH-CNC) with 0.3 wt% GO suspensions (Table 2). The proportion of CNC was analyzed from nitrogen contents in filaments (Table 2). There was also trace amount of nitrogen in GO because $NaNO_3$ was used in GO synthesis (Hummers' method), but the N content was very low and was not taken account in calculations. The GT-CNC and AH-CNC contents were very different, being 45.6 wt% and 16.0 wt% in the composite filaments, respectively. The lower content of AH-CNC was probably due to its notable higher cationic charge density. Because the complexation was based on charge interaction/neutralization, a smaller amount of CNC with high charge density was required to form a neutral complex.

3.6. Fabrication of reduced AH-CNC/GO (AH-CNC/rGO) filament

To study the potential application of these fabricated hybrid CNC/GO filaments for electronics, a preliminary study to prepare conductive filament using CNC/GO filament was conducted. AH-CNC/GO filament was chosen as an example and chemically reduced using HI as a reducing agent. The morphology, electrical and mechanical property of reduced AH-CNC/GO filament were investigated. Fig. 5 (a-f) shows the SEM images of reduced AH-CNC/GO filament (AH-CNC/rGO). The AH-CNC/rGO filament displayed a similar structure with AH-CNC/GO filament both in longitudinal and transverse direction. The fibrillar outline of CNC could still be observed distributing randomly on the surface of reduced filament. The layered rGO flakes were identified in the cross-sectional area (Fig. 5f) but displayed a looser structure compared with the compact layered GO sheets in AH-CNC/GO filament (Fig. 4i). This altered structure was probably due to the partial removal of the oxygen-containing groups from the GO sheet surface [53]. In other words, cationic AH-CNC acted as an "adhesive" and bonded the adjacent GO nanosheets together via electrostatic interaction before reduction. After HI reduction, carboxylic group was partly reduced, the interactions

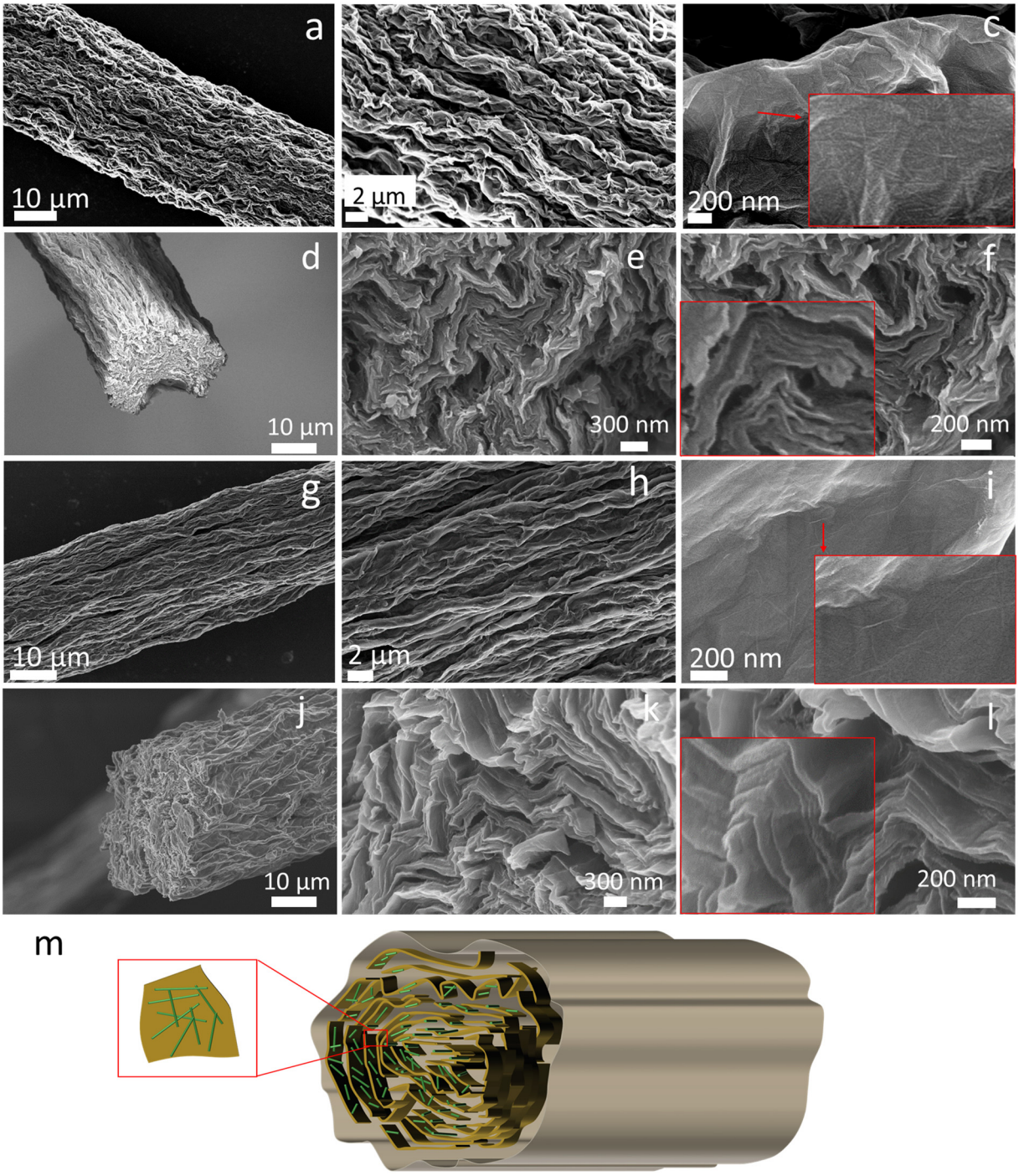

Fig. 4. The side view and cross-sectional SEM images of (a-f) GT-CNC/GO and (g-l) AH-CNC/GO filaments and the scheme of potential structure of CNC/GO hybrid filament.

between AH-CN and GO decreased forming a relatively less dense structure than GO fiber. This structure was also supported by the higher strain value of AH-CNC/rGO hybrid filament (5.6%) compared to the strain (1.8%) of original AH-CNC/GO filament. Due to the reduction of the oxygen containing functional groups of GO, AH-CNC/rGO filament showed a much higher thermal stability (<17% weight loss at 700 °C) than unreduced AH-CNC/GO filament (about 53% weight loss at 700 °C) (Fig.S6 in Supplementary Information). The average tensile strength of AH-CNC/rGO hybrid filament also increased to 109.3 ± 8 MPa, which was about 25% better compared with the original filament (87.1 MPa). This enhancement in tensile strength was presumably associated with the intrinsic higher mechanical properties (lower interlayer space) of reduced GO sheets compared to GO sheets [54,55].

Table 2
Elemental analysis of Nitrogen content in GT-CNC, GO, AH-CNC and their corresponding CNC/GO hybrid filament.

Sample	GT-CNC	AH-CNC	GO	GT-CNC/GO	AH-CNC/GO
N (wt%)	4.6 ± 0.1	15.6 ± 0.2	0.05 ± 0.01	2.1 ± 0.1	2.5 ± 0.1

The reducing treatment played an important role in restoring the electrical conductivity of the GO sheet. AH-CNC/rGO hybrid filament had an electrical conductivity of 3298 ± 167 S/m. Using the AH-CNC/

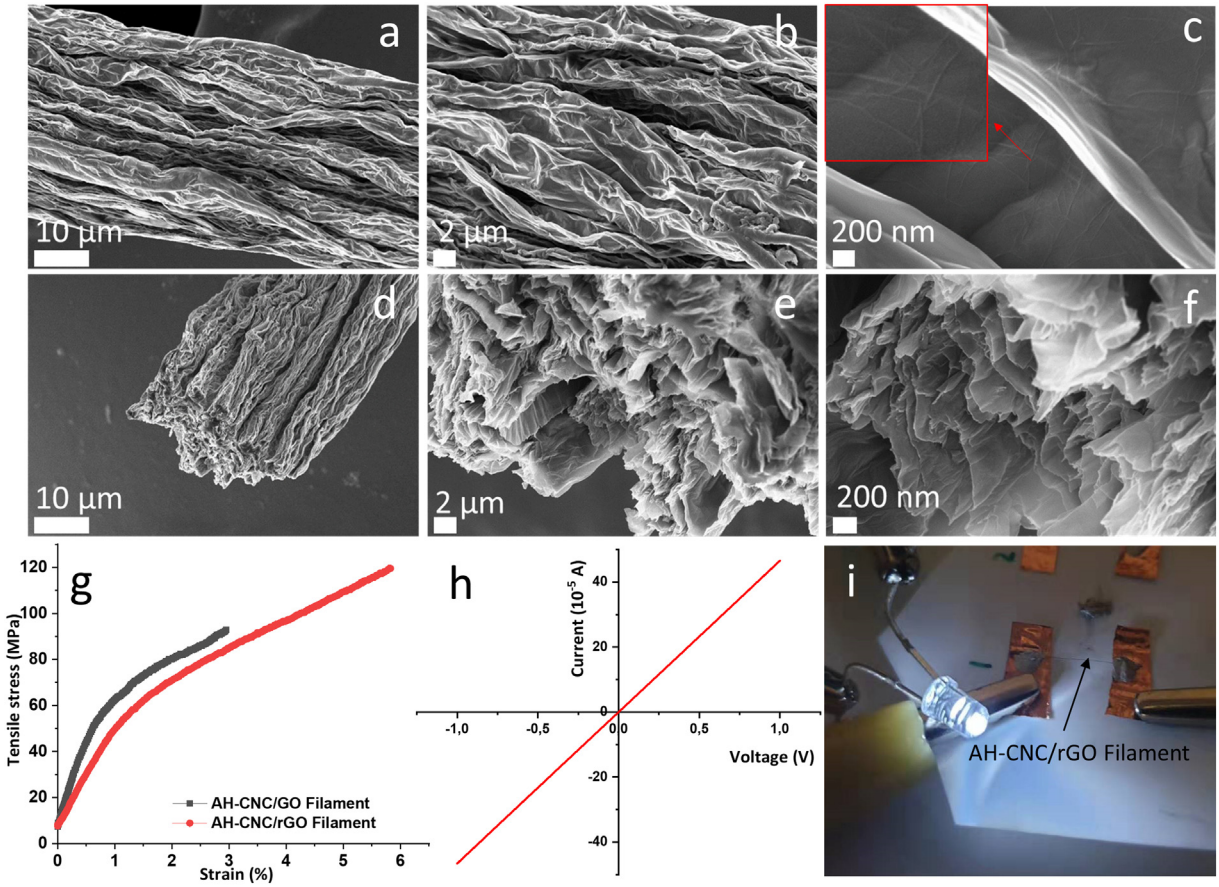

Fig. 5. Surface and cross sectional SEM images (a-f) of AH-CNC/rGO filament; (g) typical strain-stress curves of the single AH-CNC/GO and AH-CNC/rGO hybrid filament; (h) typical *I-V* curve of the single AH-CNC/rGO filament; (i) lighted LED lamp using the prepared AH-CNC/rGO filament as the leads in the electrical circuit.

rGO hybrid filament as leads in an electrical circuit, its conductance is sufficient for lighting up a LED lamp (Fig. 5i). Even though the reduced AH-CNC/GO filaments showed a lower mechanical properties compared to previously reported filaments based traditional wet spinning method (Table S1), we believe that the mechanical properties of CNC/GO filaments can further be improved by post-treatments, such as stretching or high-temperature graphitization [13,56,57]. Overall, the invented approach presents, a new facile and green technique for the assembly of 2D nanosheets with 1D nanomaterials [58]. The incorporation of additional nanoparticles and small molecules could further enable to tailor the features of filaments for other applications [41].

4. Conclusion

In conclusion, organic-inorganic nanoparticle hybrid filaments were successfully spun from cationic CNC and anionic GO via interfacial nanoparticle complexation. This process was conducted in aqueous condition and at room temperature without using any organic coagulants, thus being green and simple. Conductive CNC/rGO filament was further obtained from reduced GO, showing an improved tensile strength of 109.3 ± 8 MPa and an electrical conductivity of 3298 ± 167 S/m. The results help understanding the interactions between nanocellulose and graphene sheets for designing a NC and GO based macroscopic, assembled hybrid architectures. Additional components such as nanoparticles and small molecules can easily be integrated to the filament structure for further tailoring of material properties. This simple and versatile assembly method opens pathways to many exciting superstructures between 2D nanosheets and 1D nanocrystals or nanofibers.

Supplementary data to this article can be found online at https://doi.org/10.1016/j.matdes.2020.108791.

CRediT authorship contribution statement

Kaitao Zhang: Conceptualization, Methodology, Writing - original draft, Formal analysis. **Lukas Ketterle:** Formal analysis, Investigation. **Topias Järvinen:** Formal analysis, Writing - review & editing. **Gabriela Simone Lorite:** Formal analysis, Writing - review & editing. **Shu Hong:** Formal analysis. **Henrikki Liimatainen:** Writing - review & editing, Project administration, Funding acquisition, Supervision.

Declaration of competing interest

The authors declare that they have no known competing financial interests or personal relationships that could have appeared to influence the work reported in this paper.

Acknowledgements

The authors acknowledge the support from the Academy of Finland project "Bionanochemicals" (298295) and European Regional Development Fund/Council of Oulu region ("Novidam" project). We also thank the support of the Centre for Material Analysis in University of Oulu, Elisa Wirkkala for technical assistance in elemental analysis.

References

[1] G. Eda, M. Chhowalla, Chemically derived graphene oxide: towards large-area thin-film electronics and optoelectronics, Adv. Mater. 22 (22) (2010) 2392–2415.
[2] J. Zhu, D. Yang, Z. Yin, Q. Yan, H. Zhang, Graphene and graphene-based materials for energy storage applications, Small 10 (17) (2014) 3480–3498.
[3] H. Jiang, Chemical preparation of graphene-based nanomaterials and their applications in chemical and biological sensors, Small 7 (17) (2011) 2413–2427.

[4] X. Hu, W. Xu, L. Zhou, Y. Tan, Y. Wang, S. Zhu, J. Zhu, Tailoring graphene oxide-based aerogels for efficient solar steam generation under one Sun, Adv. Mater. 29 (5) (2017) 1604031.
[5] F. Liu, T.S. Seo, A controllable self-assembly method for large-scale synthesis of graphene sponges and free-standing graphene films, Adv. Funct. Mater. 20 (12) (2010) 1930–1936.
[6] G. Huang, C. Hou, Y. Shao, H. Wang, Q. Zhang, Y. Li, M. Zhu, Highly strong and elastic graphene fibres prepared from universal graphene oxide precursors, Sci Rep-Uk 4 (2014) 4248.
[7] K.W. Putz, O.C. Compton, C. Segar, Z. An, S.T. Nguyen, L.C. Brinson, Evolution of order during vacuum-assisted self-assembly of graphene oxide paper and associated polymer nanocomposites, ACS Nano 5 (8) (2011) 6601–6609.
[8] S. Wang, L. Yang, Q. Wang, Y. Fan, J. Shang, S. Qiu, J. Li, W. Zhang, X. Wu, Supramolecular self-assembly of layer-by-layer graphene film driven by the synergism of π–π and hydrogen bonding interaction, J. Photochem. Photobiol. A Chem. 355 (2018) 249–255.
[9] C.-C. Ji, M.-W. Xu, S.-J. Bao, C.-J. Cai, Z.-J. Lu, H. Chai, F. Yang, H. Wei, Self-assembly of three-dimensional interconnected graphene-based aerogels and its application in supercapacitors, J Colloid Interf Sci 407 (2013) 416–424.
[10] Y. Qian, I.M. Ismail, A. Stein, Ultralight, high-surface-area, multifunctional graphene-based aerogels from self-assembly of graphene oxide and resol, Carbon 68 (2014) 221–231.
[11] S.R. Shin, C. Zihlmann, M. Akbari, P. Assawes, L. Cheung, K. Zhang, V. Manoharan, Y.S. Zhang, M. Yüksekkaya, K.-t. Wan, M. Nikkhah, M.R. Dokmeci, X. Tang, A. Khademhosseini, Reduced graphene oxide-GelMA hybrid hydrogels as scaffolds for cardiac tissue engineering, Small 12 (27) (2016) 3677–3689.
[12] Y. Zhang, J. Peng, M. Li, E. Saiz, S.E. Wolf, Q. Cheng, Bioinspired supertough graphene fiber through sequential interfacial interactions, ACS Nano 12 (9) (2018) 8901–8908.
[13] Z. Xu, Y. Liu, X. Zhao, L. Peng, H. Sun, Y. Xu, X. Ren, C. Jin, P. Xu, M. Wang, C. Gao, Ultrastiff and strong graphene fibers via full-scale synergetic defect engineering, Adv. Mater. 28 (30) (2016) 6449–6456.
[14] C. Wu, X. Wang, Q. Zhuo, J. Sun, C. Qin, J. Wang, L. Dai, A facile continuous wet-spinning of graphene oxide fibers from aqueous solutions at high pH with the introduction of ammonia, Carbon 138 (2018) 292–299.
[15] B. Fang, L. Peng, Z. Xu, C. Gao, Wet-spinning of continuous montmorillonite-graphene fibers for fire-resistant lightweight conductors, ACS Nano 9 (5) (2015) 5214–5222.
[16] Z. Xu, C. Gao, Graphene chiral liquid crystals and macroscopic assembled fibres, Nat. Commun. 2 (1) (2011) 571.
[17] F. Meng, W. Lu, Q. Li, J.-H. Byun, Y. Oh, T.-W. Chou, Graphene-based fibers: a review, Adv. Mater. 27 (35) (2015) 5113–5131.
[18] W.K. Chee, H.N. Lim, Z. Zainal, N.M. Huang, I. Harrison, Y. Andou, Flexible graphene-based supercapacitors: a review, J. Phys. Chem. C 120 (8) (2016) 4153–4172.
[19] N. He, W. Shan, J. Wang, Q. Pan, J. Qu, G. Wang, W. Gao, Mordant inspired wet-spinning of graphene fibers for high performance flexible supercapacitors, J. Mater. Chem. A 7 (12) (2019) 6869–6876.
[20] H. Ahmad, M.Z. Fan, D. Hui, Graphene oxide incorporated functional materials: a review, Compos Part B-Eng 145 (2018) 270–280.
[21] L. Shang, Y. Yu, Y. Liu, Z. Chen, T. Kong, Y. Zhao, Spinning and applications of bioinspired Fiber systems, ACS Nano 13 (3) (2019) 2749–2772.
[22] N. Lin, A. Dufresne, Nanocellulose in biomedicine: current status and future prospect, Eur. Polym. J. 59 (2014) 302–325.
[23] R. Xiong, K. Hu, A.M. Grant, R. Ma, W. Xu, C. Lu, X. Zhang, V.V. Tsukruk, Ultrarobust transparent cellulose nanocrystal-graphene membranes with high electrical conductivity, Adv. Mater. 28 (7) (2016) 1501–1509.
[24] J. Xing, P. Tao, Z. Wu, C. Xing, X. Liao, S. Nie, Nanocellulose-graphene composites: a promising nanomaterial for flexible supercapacitors, Carbohyd Polym 207 (2019) 447–459.
[25] X. Du, Z. Zhang, W. Liu, Y. Deng, Nanocellulose-based conductive materials and their emerging applications in energy devices - a review, Nano Energy 35 (2017) 299–320.
[26] P. Laaksonen, A. Walther, J.-M. Malho, M. Kainlauri, O. Ikkala, M.B. Linder, Genetic engineering of biomimetic nanocomposites: diblock proteins, graphene, and nanofibrillated cellulose, Angew. Chem. Int. Ed. 50 (37) (2011) 8688–8691.
[27] R. Xiong, H.S. Kim, L. Zhang, V.F. Korolovych, S. Zhang, Y.G. Yingling, V.V. Tsukruk, Wrapping nanocellulose nets around graphene oxide sheets, Angew. Chem. 130 (28) (2018) 8644–8649.
[28] Y.B. Pottathara, V. Bobnar, M. Finšgar, Y. Grohens, S. Thomas, V. Kokol, Cellulose nanofibrils-reduced graphene oxide xerogels and cryogels for dielectric and electrochemical storage applications, Polymer 147 (2018) 260–270.
[29] J.-M. Malho, P. Laaksonen, A. Walther, O. Ikkala, M.B. Linder, Facile method for stiff, tough, and strong nanocomposites by direct exfoliation of multilayered graphene into native nanocellulose matrix, Biomacromolecules 13 (4) (2012) 1093–1099.
[30] Y. Li, H. Zhu, F. Shen, J. Wan, X. Han, J. Dai, H. Dai, L. Hu, Highly conductive microfiber of graphene oxide templated carbonization of nanofibrillated cellulose, Adv. Funct. Mater. 24 (46) (2014) 7366–7372.
[31] F.Z. Wang, L.T. Drzal, Y. Qin, Z.X. Huang, Multifunctional graphene nanoplatelets/cellulose nanocrystals composite paper, Compos Part B-Eng 79 (2015) 521–529.
[32] C. Zhu, S. Monti, A.P. Mathew, Cellulose nanofiber–graphene oxide biohybrids: disclosing the self-assembly and copper-ion adsorption using advanced microscopy and ReaxFF simulations, ACS Nano 12 (7) (2018) 7028–7038.
[33] P. Liu, C.T. Zhu, A.P. Mathew, Mechanically robust high flux graphene oxide - nanocellulose membranes for dye removal from water, J. Hazard. Mater. 371 (2019) 484–493.
[34] C. Yan, J. Wang, W. Kang, M. Cui, X. Wang, C.Y. Foo, K.J. Chee, P.S. Lee, Highly stretchable piezoresistive graphene–nanocellulose nanopaper for strain sensors, Adv. Mater. 26 (13) (2014) 2022–2027.
[35] Y. Li, H. Zhu, S. Zhu, J. Wan, Z. Liu, O. Vaaland, S. Lacey, Z. Fang, H. Dai, T. Li, L. Hu, Hybridizing wood cellulose and graphene oxide toward high-performance fibers, Npg Asia Mater 7 (1) (2015) e150.
[36] M. Mo, C. Chen, H. Gao, M. Chen, D. Li, Wet-spinning assembly of cellulose nanofibers reinforced graphene/polypyrrole microfibers for high performance fiber-shaped supercapacitors, Electrochim. Acta 269 (2018) 11–20.
[37] N. Sheng, S. Chen, J. Yao, F. Guan, M. Zhang, B. Wang, Z. Wu, P. Ji, H. Wang, Polypyrrole@TEMPO-oxidized bacterial cellulose/reduced graphene oxide macrofibers for flexible all-solid-state supercapacitors, Chem. Eng. J. (2019) 1022–1032.
[38] G. Chen, T. Chen, K. Hou, W. Ma, M. Tebyetekerwa, Y. Cheng, W. Weng, M. Zhu, Robust, hydrophilic graphene/cellulose nanocrystal fiber-based electrode with high capacitive performance and conductivity, Carbon 127 (2018) 218–227.
[39] B. Fang, D. Chang, Z. Xu, C. Gao, A review on graphene fibers: expectations, advances, and prospects, Adv. Mater. 32 (5) (2020), 1902664.
[40] K. Zhang, H. Liimatainen, Hierarchical assembly of nanocellulose-based filaments by interfacial complexation, Small 14 (38) (2018) 1801937.
[41] K. Zhang, S.D. Hujaya, T. Jarvinen, P. Li, T. Kauhanen, M.V. Tejesvi, K. Kordas, H. Liimatainen, Interfacial nanoparticle complexation of oppositely charged nanocelluloses into functional filaments with conductive, drug release, or antimicrobial property, ACS Appl. Mater. Interfaces 12 (1) (2020) 1765–1774.
[42] J. Zou, F. Kim, Self-assembly of two-dimensional nanosheets induced by interfacial polyionic complexation, ACS Nano 6 (12) (2012) 10606–10613.
[43] K. Lee, M. Do, Y.C. Seo, H. Lee, Wet-to-dry hybrid spinning of graphene fiber inspired by spider silk production mechanisms, Adv. Mater. Interfaces 5 (21) (2018), 1800585.
[44] L. Geng, Y. Lin, S. Chen, S. Shi, Y. Cai, L. Li, X. Peng, Superior strength and toughness of graphene/chitosan fibers reinforced by interfacial complexation, Compos. Sci. Technol. 194 (2020), 108174. .
[45] J.A. Sirviö, A.K. Anttila, A.M. Pirttilä, H. Liimatainen, I. Kilpeläinen, J. Niinimäki, O. Hormi, Cationic wood cellulose films with high strength and bacterial anti-adhesive properties, Cellulose 21 (5) (2014) 3573–3583.
[46] J. Ojala, J.A. Sirviö, H. Liimatainen, Nanoparticle emulsifiers based on bifunctionalized cellulose nanocrystals as marine diesel oil-water emulsion stabilizers, Chem. Eng. J. 288 (2016) 312–320.
[47] P. Li, J.A. Sirviö, B. Asante, H. Liimatainen, Recyclable deep eutectic solvent for the production of cationic nanocelluloses, Carbohyd Polym 199 (2018) 219–227.
[48] J. Sirviö, A. Honka, H. Liimatainen, J. Niinimäki, O. Hormi, Synthesis of highly cationic water-soluble cellulose derivative and its potential as novel biopolymeric flocculation agent, Carbohyd Polym 86 (1) (2011) 266–270.
[49] H. Liimatainen, T. Suopajärvi, J. Sirviö, O. Hormi, J. Niinimäki, Fabrication of cationic cellulosic nanofibrils through aqueous quaternization pretreatment and their use in colloid aggregation, Carbohyd Polym 103 (1) (2014) 187–192.
[50] H. Liimatainen, M. Visanko, J.A. Sirviö, O.E.O. Hormi, J. Niinimaki, Enhancement of the nanofibrillation of wood cellulose through sequential periodate-chlorite oxidation, Biomacromolecules 13 (5) (2012) 1592–1597.
[51] R. Kabiri, H. Namazi, Nanocrystalline cellulose acetate (NCCA)/graphene oxide (GO) nanocomposites with enhanced mechanical properties and barrier against water vapor, Cellulose 21 (5) (2014) 3527–3539.
[52] L. Bekale, D. Agudelo, H.A. Tajmir-Riahi, Effect of polymer molecular weight on chitosan–protein interaction, Colloids Surf. B: Biointerfaces 125 (2015) 309–317.
[53] S. Pei, H.-M. Cheng, The reduction of graphene oxide, Carbon 50 (9) (2012) 3210–3228.
[54] C. Lee, X. Wei, J.W. Kysar, J. Hone, Measurement of the elastic properties and intrinsic strength of monolayer graphene, Science 321 (5887) (2008) 385–388.
[55] D. Zhang, L. Peng, N. Shi, Y. Yu, Y. Min, A.J. Epstein, Self-assembled high-performance graphene oxide fibers using ionic liquid as coagulating agent, J. Mater. Sci. 52 (13) (2017) 7698–7708.
[56] G. Xin, T. Yao, H. Sun, S.M. Scott, D. Shao, G. Wang, J. Lian, Highly thermally conductive and mechanically strong graphene fibers, Science 349 (6252) (2015) 1083–1087.
[57] Z. Xu, H. Sun, X. Zhao, C. Gao, Ultrastrong fibers assembled from giant graphene oxide sheets, Adv. Mater. 25 (2) (2013) 188–193.
[58] R. Jalili, S.H. Aboutalebi, D. Esrafilzadeh, R.L. Shepherd, J. Chen, S. Aminorroaya-Yamini, K. Konstantinov, A.I. Minett, J.M. Razal, G.G. Wallace, Scalable one-step wet-spinning of graphene fibers and yarns from liquid crystalline dispersions of graphene oxide: towards multifunctional textiles, Adv. Funct. Mater. 23 (43) (2013) 5345–5354.